REPORTS

GEOPHYSICS

Tomography reveals buoyant asthenosphere accumulating beneath the Juan de Fuca plate

William B. Hawley,[1,2]* Richard M. Allen,[1,2] Mark A. Richards[1]

The boundary between Earth's strong lithospheric plates and the underlying mantle asthenosphere corresponds to an abrupt seismic velocity decrease and electrical conductivity increase with depth, perhaps indicating a thin, weak layer that may strongly influence plate motion dynamics. The behavior of such a layer at subduction zones remains unexplored. We present a tomographic model, derived from on- and offshore seismic experiments, that reveals a strong low-velocity feature beneath the subducting Juan de Fuca slab along the entire Cascadia subduction zone. Through simple geodynamic arguments, we propose that this low-velocity feature is the accumulation of material from a thin, weak, buoyant layer present beneath the entire oceanic lithosphere. The presence of this feature could have major implications for our understanding of the asthenosphere and subduction zone dynamics.

The physical causes of the lithosphere-asthenosphere boundary (LAB), possibly representing a zone that mechanically decouples tectonic plates from the asthenospheric mantle beneath (*1*, *2*), remain poorly understood (*3*). The LAB beneath continents appears deep and somewhat obfuscated by other discontinuities (*4*, *5*), so distinguishing the LAB has been hindered by the complicated nature of deep continental structures. Oceans are tectonically simpler than continents, so both the observation and description of the LAB should be simpler there. However, because oceans are poorly instrumented, serious difficulties remain in resolving the LAB beneath oceanic lithosphere (*6*). Of particular interest is this lithosphere-asthenosphere interaction at convergent margins. The geometry of an oceanic plate changes as it dips into the mantle at a subduction zone, and the response of the uppermost mantle remains debated (*7*–*9*). New constraints on processes beneath a dipping plate may provide insights into subduction zone dynamics as well as large-scale asthenospheric flow and its role in the evolution of tectonic plates.

First arrivals of *P* waves from distant earthquakes recorded on large seismic arrays can be used to illuminate large parts of the mantle. One such array, the Cascadia Initiative (*10*), was a 4-year (2011–2015) amphibious seismic deployment that covered the Juan de Fuca plate and the Cascadia subduction zone (Fig. 1). Using 61,559 *P*-wave arrivals observed on the Cascadia Initiative, the Transportable Array, and other regional seismic networks, we generated a *P*-wave velocity model of the region through finite-frequency tomographic inversion following the method of Obrebski *et al.* (*11*). Our application of finite-frequency sensitivity kernels means that our inversion takes into account the frequency-dependent volume that is sampled by a *P* wave traveling from the source to the seismometer and obviates the need to smooth the final model. The noise characteristics of the ocean bottom seismometers (OBSs) require that we use long-period (9.1- to 12.5-s) arrivals.

Our model (CASC16-P) shows an expected north-striking, east-dipping, high-velocity (+3% *P*-wave velocity change, dV_P/V_P) Juan de Fuca slab, seen at 150 km depth as a continuous north-south structure at about 122°W between 40°N and the northern edge of our model at 50°N (Fig. 2A and fig. S14). Vertical cross sections at 47°N (Fig. 2B) and 41°N (Fig. 2C) indicate that the slab is continuous down to the transition zone at ~410 km, or deeper, consistent with previous land-based studies in the region (*11*–*14*). A previously unidentified strong low-velocity anomaly (–2 to –3% dV_P/V_P) is seen at 150 km depth with similar strike as the Juan de Fuca slab, just to the west. Vertical cross sections through the models and synthetic tests (see figs. S6 and S7 and Materials and methods) indicate that this feature is restricted to the top 300 km of the model directly beneath the Juan de Fuca slab, meaning that it does not follow the slab all the way down to the transition zone. Further tests with various station correction terms (fig. S5) indicate that this feature is not a shallow structure being incorrectly mapped to depth. This truncated feature appears to take the shape of a horizontal cylinder, slightly elongated vertically in cross section beneath the high-velocity slab. The addition of data from the Cascadia Initiative has provided the offshore resolution needed to confidently identify the full extent of this feature, though evidence exists for the feature in previous land-based tomographic models of the region (*11*–*14*).

We propose that this low dV_P feature is related to previously reported observations of a layer of partial melt beneath the oceanic lithosphere. A range of techniques—including receiver functions from borehole OBSs on the Pacific and Philippine Sea plates (*15*), precursors to teleseismic SS-phase arrivals spanning the Pacific ocean (*16*), magnetotelluric inversion on the Nazca plate (*17*), and explosion-generated reflected *P* waves offshore of New Zealand (*18*)—resolve a narrow (10 to 25 km) region, immediately below the oceanic lithosphere, characterized by low seismic wave velocities (–6 to –10% dV_S/V_S and dV_P/V_P) and high conductivity (4 to 6 ohm·m). The interpretation for each of these studies is slightly different, but they all indicate that partial melt fractions of ~1 to 4% in the uppermost asthenosphere are consistent with their findings, with variations arising due to different geometries of melt layers, composition of the melt, and the crystal structure of the materials in the layer. The slow seismic feature we observe in CASC16-P similarly coincides with a region of high conductivity. This thin layer is not resolvable in tomographic studies that use relative travel times from teleseismic events (*11*–*13*) because such variations affect each ray path in the same way (*19*). At a subduction zone, however, this layer might become observable where it changes geometry with the slab as it descends, thus becoming detectable via teleseismic body-wave tomography.

Predicting a priori how this layer might behave beneath a subduction zone requires knowledge of its physical properties. Because we cannot resolve the layer to the west of the subduction zone, CASC16-P does not provide a direct observation of the source of the material in this layer. Previous reports (*15*–*18*) attribute the layer to volatiles and/or hydrated mantle increasing partial melt fraction in the uppermost asthenosphere, decreasing density and viscosity, separating into lenses (*20*) or channels (*15*, *21*), and ponding beneath the rigid, impermeable lithospheric lid (*22*). Our observations, as well as the land-based observation of a high-conductivity region that roughly coincides with our low velocities (*23*), could be explained by the accumulation of material from this horizontal layer due to its own buoyancy and low viscosity.

Here we use two straightforward fluid-mechanical scaling calculations to demonstrate the plausibility of the accumulation hypothesis: First, for a thin, buoyant, low-viscosity layer to accumulate beneath the downgoing slab the ratio of the upward mass flux due to the layer buoyancy (Poiseuille flow) must exceed the downward flux due to drag from the downgoing slab (Couette flow) (*24*). Referring to the notation in Fig. 3, this means that

$$\frac{\Delta\rho g \sin(\theta) h^2}{6 v_0 \mu_1} \gtrsim 1 \qquad (1)$$

Here, Δρ is the difference in density, *g* is gravitational acceleration, θ is the dip angle, *h* is the

[1]Department of Earth and Planetary Science, University of California, Berkeley, Berkeley, CA 94720, USA. [2]Berkeley Seismological Laboratory, 215 McCone Hall, University of California, Berkeley, Berkeley, CA 94720, USA.
*Corresponding author. Email: whawley@seismo.berkeley.edu

layer thickness, v_0 is the plate velocity, and μ_l is the thin-layer viscosity. The second condition is that the horizontal gravitational spreading velocity of the accumulated low-velocity volume due to its own buoyancy cannot exceed the horizontal advection velocity due to plate motion (*25*), otherwise the accumulating low-viscosity body would spread out instead of accumulating to the observed thickness of $H \approx 50$ to 100 km, as inferred from our tomographic images. This means that

$$\frac{\Delta\rho g H^2}{v_0 \mu_m} \lesssim 1 \qquad (2)$$

Here, H is the thickness of the accumulated material, and $\{\mu_m\}$ is the viscosity of the underlying mantle. In obtaining Eqs. 1 and 2, we assumed that the thin-layer viscosity controlling return flow is much smaller than the underlying mantle viscosity governing gravitational spreading—that is, $\mu_l \ll \mu_m$ (see supplementary materials for details).

Assuming that $\Delta\rho \approx 5$ to 20 kg/m^3 [1 to 4% partial melt, with 500 kg/m^3 density contrast between melt and solid (*26*)], $g = 9.8$ m/s^2, $\theta = 40°$,

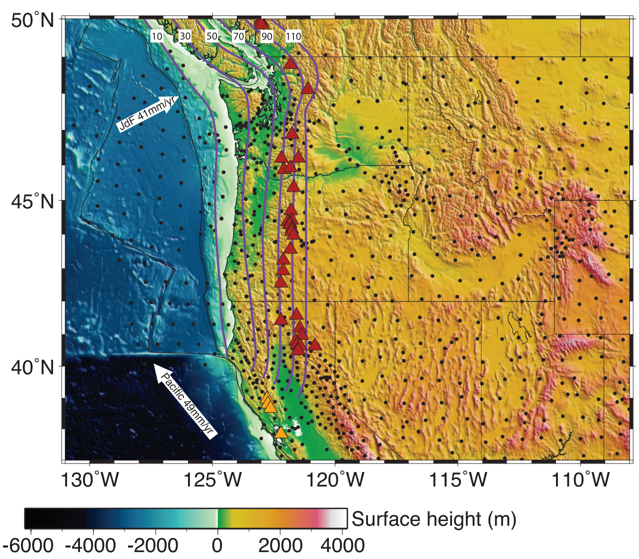

Fig. 1. Stations used in our inversion (black dots) overlain on topography. Cascade volcanoes are denoted by red triangles, and northward age-progressive volcanism of the California Coast Ranges is shown by orange triangles. White arrows indicate plate motions relative to North America. The estimated depth of the top of the subducting slab is shown by the purple contours labeled in kilometers (*36*).

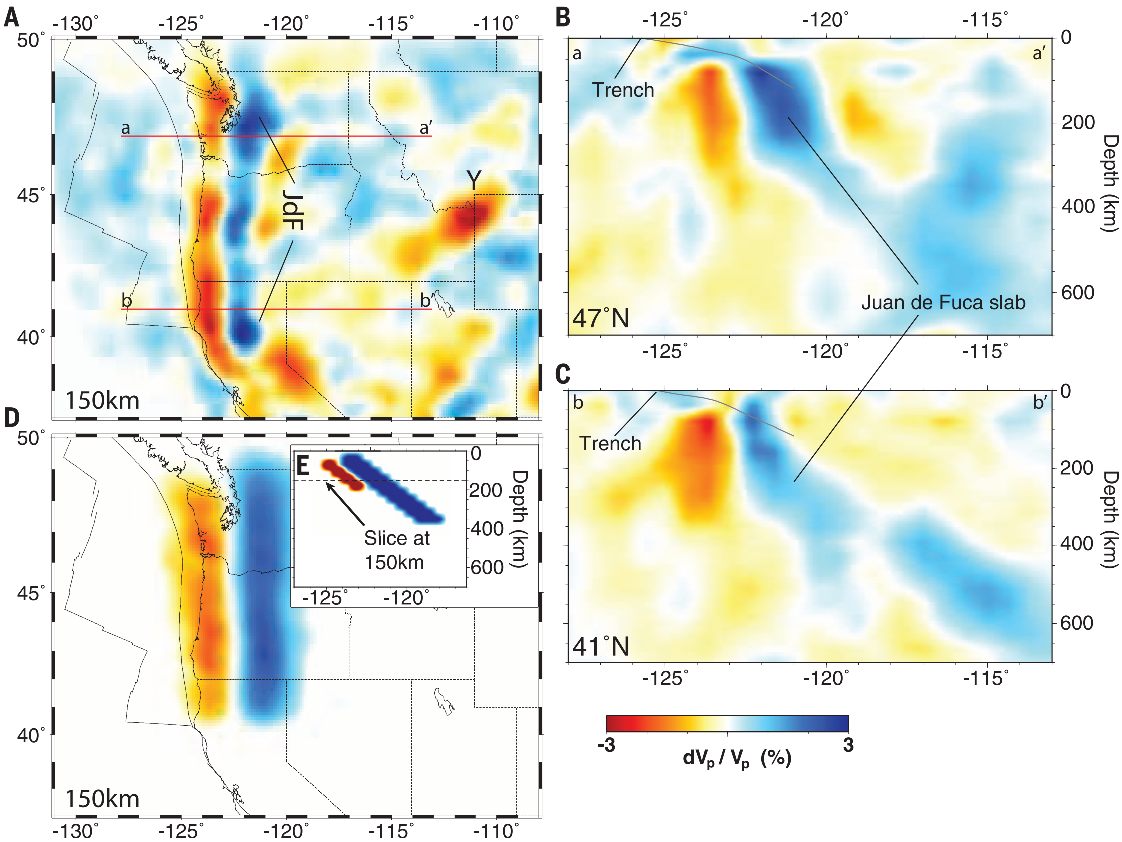

Fig. 2. Slices through CASC16-P. (**A**) A slice at 150 km depth. The slow Yellowstone (Y) and fast Juan de Fuca (JdF) slab anomalies are indicated. A strong low-velocity anomaly is seen west of the Juan de Fuca slab. Lines a-a′ and b-b′ mark the locations of vertical slices through CASC16-P at 47°N (**B**) and 41°N (**C**). These slices show the slab extending through the transition zone, whereas the low-velocity anomaly is confined to shallower depths (<~300 km). The top of the slab (*36*) is shown with a gray line that begins at the trench. There is no vertical exaggeration in the vertical slices. (**D**) A slice at 150 km depth shows the recovery of a synthetic test with a 120-km-thick +4% slab anomaly underlain by a 40-km-thick –10% layer anomaly. The input synthetic velocity model is shown in (**E**). The recovery of synthetic features (D) is similar to that observed (A).

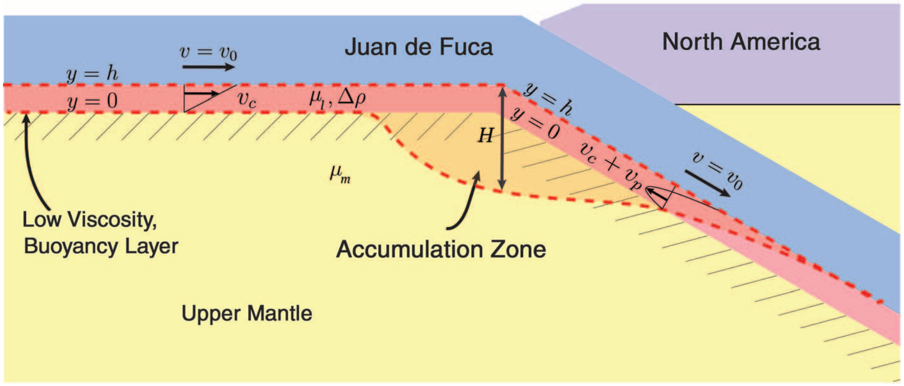

Fig. 3. Geodynamical model setup. The low-velocity layer in red (of thickness h) lies between the Juan de Fuca plate in blue and the asthenosphere in yellow. Comparison of the Couette and Poiseuille velocity terms (v_c and v_p, each as a function of y, the distance from the top of the upper mantle) yields an estimate for the viscosity of this layer (μ_l). In reality, this structure may take the shape outlined by the red dashed lines and tinted orange: thicker beneath the trench and thinning out with depth. The extent of this feature depends on the density difference ($\Delta\rho$) and the upper mantle viscosity (μ_m). The features in this model are not to scale.

v_0 = 40 mm/year, and $h \approx 10$ to 25 km, Eq. 1 implies that the viscosity of the thin, weak layer falls in the range $\mu_l \approx 0.04$ to 1.0×10^{19} Pa·s, which is reasonable for partially molten uppermost mantle (*27*). Similarly, with a low-velocity feature thickness of $H \approx 50$ to 100 km, Eq. 2 yields an underlying mantle viscosity that falls in the range $\mu_m \gtrsim 0.1$ to 1.5×10^{21} Pa·s, which is also reasonable (*27*, *28*). Furthermore, a convergence rate of ~40 mm/year indicates that about 100 to 400 km of continuous subducted lithosphere would be required to form the observed feature from accumulation of a thin buoyant, sublithospheric layer, a condition consistent with the ~400 km of continuous slab observed in our tomographic model.

A more sophisticated treatment of this interesting mantle flow problem is beyond the scope of this paper, requiring a full numerical solution to understand the balance of Couette- and Poiseuille-type flow within the asthenosphere (*29*), as well as consideration of other complicating factors, such as trench-parallel extrusion of buoyant material toward the slab edges (see below), relaxing the assumption that $\mu_l \ll \mu_m$, etc. However, satisfaction of the two necessary conditions above for accumulation and maintenance of the low-velocity feature demonstrates that our hypothesis is plausible. More precise knowledge of the geometry of the feature will help constrain critical physical parameters, but CASC16-P provides a maximum extent of the feature. The grid we used in the inversion and the smoothing due to finite-frequency sensitivity kernels make a strong, thin velocity anomaly appear thicker and weaker (Fig. 2, D and E). Further studies with higher resolution will enable more detailed geodynamical models.

The material we observe could be important for "petit spot" volcanism in the forearc bulge east of the Japan trench. Samples from these young (~5-million-year-old), alkalic volcanoes in the 120-million- to 150-million-year-old Pacific plate (notably much older than any part of the Juan de Fuca plate) are highly vesicular, suggesting the presence of CO_2, and isotopically similar to basalts found at mid-ocean ridges. One explanation for the presence of these volcanoes in such an unusual region of the ocean floor is that the volcanism is due to partial melt rising through flexure-induced fractures in the lithosphere and that it lends credence to the idea that the asthenosphere is a zone of partial melt (*30*). Other studies (*26*, *31*) argue that the entire asthenosphere need not be a zone of partial melt. The proposed low-viscosity layer could provide a source for enigmatic volcanism without requiring any assumptions of partial melt throughout the asthenosphere. Additionally, the chemistry of such basalts may help contextualize the composition of the low-viscosity layer.

This potentially somewhat molten feature may also explain the anomalous heat flow and volcanism of the Coast Ranges of California (orange triangles in Fig. 1). Lachenbruch and Sass (*32*) proposed that as the southern edge of the Juan de Fuca slab migrates northward with the Mendocino Triple Junction, the "window" that opens beneath the margin of North America is filled with asthenosphere that undergoes decompression melting, thus leading to high heat flow and volcanism. Seismic observations (*33*, *34*) reveal a high-velocity layer at the base of the North American crust beneath the California Coast Ranges. The thickness of this inferred mafic structure requires more melt than predicted by standard asthenospheric upwelling models. Both the lack of high-grade metamorphism inferred from the same seismic studies and the heat flow observations of Lachenbruch and Sass (*32*) indicate less heat than predicted from the same asthenospheric upwelling models (*33*). A mechanism to generate more melt at lower temperatures has been elusive, but the accumulated low-velocity, partially molten, and/or high volatile content material that we have imaged may provide that mechanism—that is, decompression of the accumulated, already partially molten feature as it emerges toward the south through the slab window would provide more melt at lower temperatures.

REFERENCES AND NOTES

1. M. A. Richards, W.-S. Yang, J. R. Baumgardner, H.-P. Bunge, *Geochem. Geophys. Geosyst.* **2**, 1026 (2001).
2. C. H. Craig, D. McKenzie, *Earth Planet. Sci. Lett.* **78**, 420–426 (1986).
3. K. M. Fischer, H. A. Ford, D. L. Abt, C. A. Rychert, *Annu. Rev. Earth Planet. Sci.* **38**, 551–575 (2010).
4. C. A. Rychert, P. M. Shearer, *Science* **324**, 495–498 (2009).
5. H. Yuan, B. Romanowicz, K. M. Fischer, D. Abt, *Geophys. J. Int.* **184**, 1237–1260 (2011).
6. H. Kawakatsu, *Science* **335**, 1448–1449 (2012).
7. T.-R. A. Song, H. Kawakatsu, *Geophys. Res. Lett.* **39**, L17301 (2012).
8. M. D. Long, P. G. Silver, *Science* **319**, 315–318 (2008).
9. M. D. Long, P. G. Silver, *Surv. Geophys.* **30**, 407–461 (2009).
10. D. Toomey *et al.*, *Oceanography* **27**, 138–150 (2014).
11. M. Obrebski, R. M. Allen, M. Xue, S.-H. Hung, *Geophys. Res. Lett.* **37**, L14305 (2010).
12. B. Schmandt, E. Humphreys, *Earth Planet. Sci. Lett.* **297**, 435–445 (2010).
13. Y. Tian, D. Zhao, *Phys. Earth Planet. Inter.* **200–201**, 72–84 (2012).
14. R. W. Porritt, R. M. Allen, F. F. Pollitz, *Earth Planet. Sci. Lett.* **402**, 16–25 (2014).
15. H. Kawakatsu *et al.*, *Science* **324**, 499–502 (2009).
16. N. Schmerr, *Science* **335**, 1480–1483 (2012).
17. S. Naif, K. Key, S. Constable, R. L. Evans, *Nature* **495**, 356–359 (2013).
18. T. A. Stern *et al.*, *Nature* **518**, 85–88 (2015).
19. I. D. Bastow, *Geophys. J. Int.* **190**, 1271–1278 (2012).
20. M. M. Hirschmann, *Phys. Earth Planet. Inter.* **179**, 60–71 (2010).
21. W. Zhu, G. A. Gaetani, F. Fusseis, L. G. J. Montési, F. De Carlo, *Science* **332**, 88–91 (2011).
22. G. Hirth, D. L. Kohlstedt, *Earth Planet. Sci. Lett.* **144**, 93–108 (1996).
23. R. L. Evans, P. E. Wannamaker, R. S. McGary, J. Elsenbeck, *Earth Planet. Sci. Lett.* **402**, 265–274 (2014).
24. D. L. Turcotte, G. Schubert, *Geodynamics* (Cambridge Univ. Press, 2002).
25. M. A. Feighner, M. A. Richards, *Earth Planet. Sci. Lett.* **129**, 171–182 (1995).
26. S. Karato, H. Jung, *Earth Planet. Sci. Lett.* **157**, 193–207 (1998).
27. C. Doglioni, A. Ismail-Zadeh, G. Panza, F. Riguzzi, *Phys. Earth Planet. Inter.* **189**, 1–8 (2011).
28. A. Paulson, M. A. Richards, *Geophys. J. Int.* **179**, 1516–1526 (2009).
29. T. Höink, A. Lenardic, *Geophys. J. Int.* **180**, 23–33 (2010).
30. N. Hirano *et al.*, *Science* **313**, 1426–1428 (2006).
31. U. Faul, I. Jackson, *Earth Planet. Sci. Lett.* **234**, 119–134(2005).
32. A. H. Lachenbruch, J. H. Sass, *J. Geophys. Res.* **85**, 6185–6222 (1980).
33. J. A. Hole, B. C. Beaudoin, T. J. Henstock, *Tectonics* **17**, 802–818 (1998).
34. K. P. Furlong, S. Y. Schwartz, *Annu. Rev. Earth Planet. Sci.* **32**, 403–433 (2004).
35. P. Wessel, W. H. F. Smith, R. Scharroo, J. Luis, F. Wobbe, *Eos* **94**, 409–410 (2013).
36. P. A. McCrory, J. L. Blair, F. Waldhauser, D. H. Oppenheimer, *J. Geophys. Res.* **117**, B09306 (2012).

ACKNOWLEDGMENTS

Support for this work was provided by the NSF under the Graduate Research Fellowship Program (grant DGE-1106400 to W.B.H.) and grant OCE-1139701 (to W.B.H. and R.M.A.). The seismic data used in this study are archived by the Incorporated Research Institutions for Seismology Data Management Center (http://ds.iris.edu/ds/nodes/dmc/) and the Northern California Earthquake Data Center (www.ncedc.org; doi:10.7932/NCEDC). Data are provided by many networks (see the supplementary materials), but of particular note are the Cascadia Initiative ocean bottom data collected by the Ocean Bottom Seismograph Instrument Pool (www.obsip.org/) and funded by the NSF (grant OCE-1112722). The Generic Mapping Tools software (*35*) was used to create the figures.

SUPPLEMENTARY MATERIALS

www.sciencemag.org/content/353/6306/1406/suppl/DC1
Materials and Methods
Figs. S1 to S14
References (*37–42*)

9 November 2015; accepted 24 August 2016
10.1126/science.aad8104

Tomography reveals buoyant asthenosphere accumulating beneath the Juan de Fuca plate

William B. Hawley, Richard M. Allen and Mark A. Richards

(September 22, 2016)
Science **353** (6306), 1406-1408. [doi: 10.1126/science.aad8104]